International Journal of Heat and Fluid Flow 30 (2009) 1087–1098

Contents lists available at ScienceDirect

International Journal of Heat and Fluid Flow

journal homepage: www.elsevier.com/locate/ijhff

Structure of the turbulent boundary layer over a rod-roughened wall

Jae Hwa Lee [a], Seung-Hyun Lee [b], Kyoungyoun Kim [c], Hyung Jin Sung [a,*]

[a] Department of Mechanical Engineering, KAIST, 373-1 Guseong-dong, Yuseong-gu, Daejeon 305-701, Republic of Korea
[b] Korea Institute of Machinery and Materials, 104 Sinseongno, Yuseong-gu, Daejeon 305-701, Republic of Korea
[c] Department of Mechanical Engineering, Hanbat National University, San 16-1, Duckmyoung-dong, Yuseong-gu, Daejeon 305-719, Republic of Korea

ARTICLE INFO

Article history:
Received 16 May 2009
Received in revised form 22 July 2009
Accepted 30 August 2009
Available online 30 September 2009

Keywords:
Turbulent boundary layer
Direct numerical simulation
Surface roughness
Roughness sublayer
Turbulent vortical structure

ABSTRACT

Turbulent coherent structures near a rod-roughened wall are scrutinized by analyzing instantaneous flow fields obtained from direct numerical simulations (DNSs) of a turbulent boundary layer (TBL). The roughness elements used are periodically arranged two-dimensional spanwise rods, and the roughness height is $k/\delta = 0.05$ where δ is the boundary layer thickness. The Reynolds number based on the momentum thickness is varied in the range $Re_\theta = 300$–1400. The effect of surface roughness is examined by comparing the characteristics of the TBLs over smooth and rough walls. Although introduction of roughness elements onto the smooth wall affects the Reynolds stresses throughout the entire boundary layer when scaled by the friction velocity, the roughness has little effect on the vorticity fluctuations in the outer layer. Pressure-strain tensors of the transport equation for the Reynolds stresses and quadrant analysis disclose that the redistribution of turbulent kinetic energy of the rough wall is similar to that of the smooth wall, and that the roughness has little effect on the relative contributions of ejection and sweep motions in the outer layer. To elucidate the modifications of the near-wall vortical structure induced by surface roughness, we used two-point correlations, joint weighted probability density function, and linear stochastic estimation. Finally, we demonstrate the existence of coherent structures in the instantaneous flow field over the rod-roughened surface.

1. Introduction

Turbulent boundary layers (TBLs) are observed in numerous fluid dynamic engineering applications, and the characteristics of TBLs have been examined in many experimental and numerical studies. In real engineering applications involving wall-bounded boundary layer flow—for example, automobiles, ships, airplanes, and heat-exchangers—the roughness of the wall surface is an important design parameter because it influences characteristics such as the transport of heat, mass and momentum. Although the effects of surface roughness on a TBL have been examined in many experimental and numerical studies, knowledge of these effects remains incomplete.

Townsend's (1976) wall-similarity hypothesis and subsequent extensions by Raupach et al. (1991) and Jimenez (2004) state that outside the roughness sublayer turbulent motions are independent of the surface roughness, and that the interaction between the inner and outer layers is very weak at sufficiently large values of the Reynolds number normalized by the wall shear stress. In further support of this similarity hypothesis, a number of studies have found that the outer layers of flows past smooth and rough walls were similar in terms of both mean flow and turbulent statistics, consistent with Townsend's hypothesis for three-dimensional roughness. These studies include the work of Shockling et al. (2006) on a honed pipe, and the examination of sandpaper and a woven mesh by Flack et al. (2005).

Results from several experimental studies of TBLs over surfaces with two-dimensional rod roughness, however, have been contrary to the wall-similarity hypothesis. For example, in experiments on TBLs over woven mesh, transverse round rod roughness elements, Krogstad and Antonia (1999) found that introduction of roughness caused significant changes of the turbulent statistics not only in the roughness sublayer but also in the outer layer and that the interaction between the inner and outer layers was non-negligible. These experimental results oppose the notion that the outer layer of a TBL is insensitive to the surface roughness, and have led to considerable uncertainty regarding the effects of surface roughness on TBLs.

Recently, numerical studies of turbulent flow over surfaces with roughness elements showed that the wall-similarity hypothesis in the outer layer depends on which turbulent statistics are used in the analysis. Lee and Sung (2007) performed a direct numerical simulation (DNS) of the TBL over smooth or rod-roughened walls and examined the spatially developing characteristics of the rough-wall TBL. They found that when turbulent quantities are normalized by the friction velocity, rod roughness influences turbulent stresses and vertical turbulent transport not only in the

* Corresponding author. Tel.: +82 42 350 3027; fax: +82 42 350 5027.
E-mail address: hjsung@kaist.ac.kr (H.J. Sung).

0142-727X/$ - see front matter © 2009 Elsevier Inc. All rights reserved.
doi:10.1016/j.ijheatfluidflow.2009.08.002

roughness sublayer but also in the outer layer. However, they observed good wall similarity for the third-order moments and the Reynolds anisotropic tensor without using the friction velocity. Similar results were obtained by Bhaganagar et al. (2004) in a study of flow through an asymmetric channel with a rough wall at the bottom and a smooth wall at the top. Specifically, they found that the turbulent stresses in the outer layer were affected by the surface roughness but the vorticity fluctuations were similar for the smooth and rough walls. On the basis of these observations, they proposed that the inner and outer layers of the turbulent boundary layer interact at large scales but not at small scales.

There have been a few experimental attempts to investigate the roughness effects on turbulence structures. Krogstad and Antonia (1994) found that the streamwise extent of all correlations was greater for the smooth wall than that for the rough walls and that the average angle of the turbulent structure was larger over the rough walls. Flack et al. (2007) showed that the effects of roughness on the quadratic components of Reynolds shear stress are negligible in the outer layer for three-dimensional roughness. Lee et al. (2008) performed particle image velocimetry (PIV) measurements on a rough-wall TBL and compared PIV results with DNS results from Lee and Sung (2007). They showed very good agreement of turbulent statistics between PIV and DNS results in the roughness sublayer when they are normalized by free-stream velocity and roughness height. They also observed inclined vortical structures shed from the rod and strong downward sweep motion in the cavity. Furthermore, Sabot et al. (1977) found in the pipe flow with ring-shaped rod roughness that the ratio of the fractional contribution from the second to the fourth quadrant strongly depends on the wall roughness.

Several DNS studies have been conducted to investigate the roughness effects on turbulence structures for the turbulent channel with rough walls. Ashrafian and Andersson (2006) investigated the effects of surface roughness on the vorticity fluctuations and turbulent kinetic energy budgets. They found that turbulent statistics are not affected by surface roughness in the outer layer of the turbulent channel with symmetric rod-roughened walls. Ikeda and Durbin (2007) found that two-dimensional rod roughness produces three-dimensional unorganized motions of vortices. They proposed that non-periodic and irregular spanwise vortex shedding serves as energy sources for the turbulent kinetic energy flux towards the wall surface. Coceal et al. (2007) investigated coherent structures in the log-region by using two-point correlations, quadrant analysis and linear stochastic estimation (LSE). They found the presence of low-momentum regions (LMRs) and hairpin-like vortices. However, since it is known that surface roughness effects are influenced by the flow type, e.g., symmetric channel flow, asymmetric channel flow, boundary layer, pipe flow and so on (Krogstad et al., 2005), it is needed to investigate the modification of coherent structure in the turbulent boundary layer with rough wall.

In the present study, the interaction between the inner and outer layers induced by rod roughness was examined through analysis of the DNS data of Lee and Sung (2007). The roughness was composed of two-dimensional spanwise rods with square cross-section that were periodically arranged in the streamwise direction with a pitch of $\lambda/k = 8$ which has a maximum value of form drag (Leonardi et al., 2003). To examine the outer-layer similarity and the scaling parameters, vorticity fluctuations were investigated and quadrant analysis was performed. Further, to elucidate the redistribution of turbulent kinetic energy, we examined the pressure-strain tensors in the transport equations of the Reynolds stresses. Finally, two-point correlations, joint weighted probability density function, linear stochastic estimation and instantaneous flow fields were scrutinized to analyze the turbulent structures arising from surface roughness not only in the roughness sublayer but also in the outer layer.

2. Numerical method

For an incompressible flow, the non-dimensional governing equations are

$$\frac{\partial u_i}{dt} + \frac{\partial u_i u_j}{\partial x_j} = -\frac{\partial p}{\partial x_i} + \frac{1}{\mathrm{Re}}\frac{\partial^2 u_i}{\partial x_j \partial x_j} + f_i \tag{1}$$

$$\frac{\partial u_i}{\partial x_i} = 0 \tag{2}$$

where x_i are the Cartesian coordinates and u_i are the corresponding velocity components. All variables are non-dimensionalized by the free-stream velocity (U_∞) and momentum thickness at the inlet (θ_{in}), and Re is the Reynolds number. The governing equations are integrated in time using the fractional step method with the implicit velocity decoupling procedure proposed by Kim et al. (2002). Based on a block LU decomposition, both velocity–pressure decoupling and additional decoupling of intermediate velocity components are achieved through approximate factorization. Under this approach, the terms are first discretized in time using the Crank–Nicholson method, and then the coupled velocity components are solved without iteration. All terms are resolved using a second-order central difference scheme in space with a staggered mesh. In the present study, the immersed boundary method is used to describe the roughness elements with Cartesian coordinates and a rectangular domain (Kim et al., 2001). The discrete-time momentum forcing f_i is calculated explicitly in time to satisfy the no-slip condition at the immersed boundary using the previous velocity field near the forcing point.

Fig. 1 shows a schematic of the computational domain and the two-dimensional rod roughness used in the present study. The notational convention adopted is that x, y, and z denote the streamwise, vertical and spanwise coordinates and u, v, and w denote the streamwise, wall-normal and spanwise components of velocity, respectively. The computational domain in each direction ($L_x \times L_y \times L_z$) is $768\theta_{in} \times 60\theta_{in} \times 80\theta_{in}$, where the corresponding mesh size is $2049 \times 150 \times 257$. Time-dependent turbulent inflow data are provided at the inlet based on the method of Lund et al. (1998). The inlet Reynolds number based on the momentum thickness (θ_{in}) and free-stream velocity (U_∞) is $Re_{\theta,in} = 300$. A convective boundary condition at the exit has the form $(\partial u/\partial t) + c(\partial u/\partial x) = 0$, where c is the local bulk velocity. The no-slip boundary condition is imposed at the solid wall, and the boundary conditions on the top surface of the computational domain are $u = U_\infty$ and $\partial v/\partial y = \partial w/\partial y = 0$. A periodic boundary condition is applied in the spanwise direction. Non-uniform grid distributions are employed in the wall-normal direction using the hyperbolic tangent function and a uniform grid distribution in both the streamwise and spanwise directions. The mesh resolutions are $\Delta x^+ = 6.0$, $\Delta y_{min}{}^+ = 0.2$, and $\Delta z^+ = 5.0$, respectively. To avoid generating a rough-wall inflow, which is prohibitively difficult, the first rod is placed $80\theta_{in}$ downstream from the inlet, and the surface

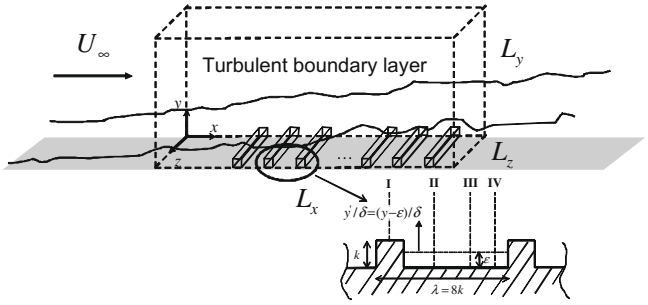

Fig. 1. Schematic of computational domain and rod roughness.

condition changes abruptly from smooth to rough at this location. The virtual origin (ϵ), which is the centroid of the momentum of the forces acting on the rod roughness, is used for the wall-normal distance from the wall. Details regarding the numerical algorithm can be found in Lee and Sung (2007).

In the present study, four selected locations (I–IV) are selected to scrutinize the coherent structures over rough wall, which are the same as those selected Ashrafian et al. (2004). Section I is located at the center of the roughness crest. Section II is located at the focal point of the primary recirculation zone downstream of the roughness element and Section III is located at the saddle-point between the two recirculation zones. Finally, Section IV is located at the focal point of the second recirculation zone.

3. Results and discussion

3.1. Mean velocity profiles

Before proceeding further, it is important to first establish the reliability and accuracy of the present numerical simulations. One of the fundamental ideas of turbulent flow is that statistical quantities at different Reynolds numbers should collapse to a single profile when normalized by the proper velocity and length scales at high Reynolds number. The mean velocity profile described by the universal logarithmic law and located between the inner and outer layers is a good example of this idea. The mean streamwise velocity distributions calculated in the present study are shown with experimental data, which used the rods having the effective roughness height k_s = 9.8 mm (Fig. 2). Locations II and IV marked in Fig. 1 are considered. Symbols are the experimental results of Krogstad and Antonia (1999) and solid lines represent the results of the present study. The numerical and experimental profiles are in satisfactory agreement. The general velocity shift (roughness function) is clearly shown and is estimated to be 9.8. The velocity defect plot shows that the rough surface profile is very similar to the smooth wall velocity profile in the outer layer, suggesting that the effects of surface roughness are restricted to the inner wall layer.

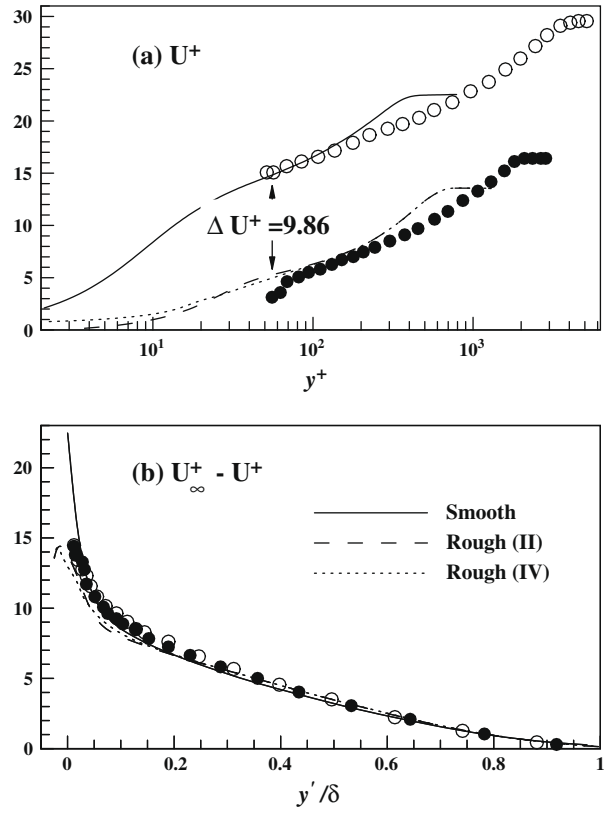

Fig. 2. (a) Mean velocity profiles and (b) mean velocity defect profiles normalized by the friction velocity.

3.2. Roughness function

Over the surface roughness, the mean streamwise velocity profile is shifted downward in the log-region by ΔU^+. The velocity distribution in the log-region for the rough-wall TBL can be expressed in the following form:

$$U^+ = \frac{1}{\kappa}\ln y^+ + B - \Delta U^+ \tag{3}$$

where $U^+ = U/u_\tau$ and $y^+ = (y-\epsilon)u_\tau/\nu$. ϵ is the distance from the wall to the virtual origin and y is measured from the bottom of the rough surface, κ is the von Karman constant and B is a smooth wall constant. Several previous studies proposed the correlation between ΔU^+ and k^+ as $\Delta U^+ = \frac{1}{\kappa}\ln k^+ + C$, where C depends on the roughness density and the shape of the roughness elements. Krogstad and Antonia (1999) suggested that for the k-type rod roughness, ΔU^+ and k^+ are related by a logarithmic function of the form $\Delta U^+ = \frac{1}{\kappa}\ln k^+ + 1.2$. Recently, Orlandi and Leonardi (2008) proposed a new simple expression by introducing the root-mean-square of the wall-normal velocity fluctuation at the plane of the crests (v'_{w^+}). They defined a slip velocity U_0 as the mean streamwise velocity at the roughness crest to normalize the streamwise mean velocity in the log-region as $\tilde{U}^+ = \frac{1}{\kappa}\ln y^+ + B - \Delta U^+$ where $\tilde{U}^+ = \frac{U-U_0}{u_\tau}$ and $\Delta U^+ = \frac{B}{\kappa}v'^+_w$. In the present study, we calculated ΔU^+ = 9.86 and $v'_{w^+} = 0.81$ from the DNS data of Lee and Sung (2007) and ΔU^+ = 10.6 and $v'_{w^+} = 0.87$ from the PIV of Lee et al. (2008), respectively. Fig. 3 shows the relation $\Delta U^+ = \frac{B}{\kappa}v'_{w^+}$ of Orlandi and Leonardi (2006, 2008). The present DNS and PIV results collapse well with the correlation of B = 5.0. Although only two cases of TBL are included in Fig. 3, we found that the formula of Orlandi and Leonardi (2008) works well in turbulent channel flow as well as in TBL.

3.3. Pressure-strain redistribution tensor

Introduction of rod roughness elements onto a smooth surface significantly affects the turbulent flow structures, leading to very high turbulent intensities in the vicinity of the wall. This near-wall region, which is known as the roughness sublayer, is generally assumed to have a height of 2–5 times the roughness height. The lim-

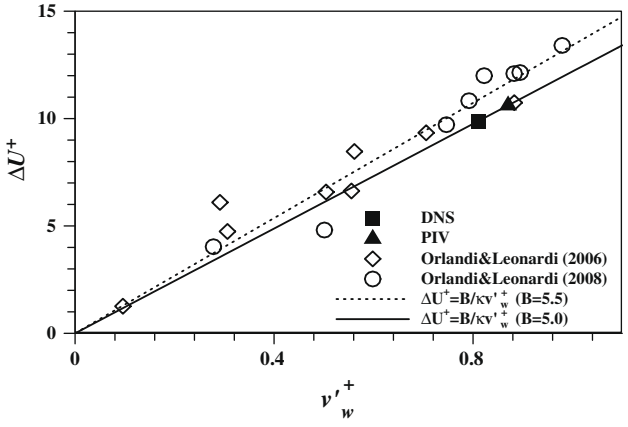

Fig. 3. Correlation between $\Delta U^+$and v'_{w^+}.

it of the roughness sublayer is defined as the point at which the turbulence statistics become spatially homogeneous (Bhaganagar et al., 2004). Schultz and Flack (2005) defined the roughness sublayer as the distance from the wall beyond which the roughness no longer has an influence on the turbulence statistics. Jimenez (2004) suggested that when δ/k is larger than 40, wall similarity can be expected and the extent of the roughness sublayer is about $5k$. Schultz and Flack (2005) proposed that k_s (the effective sand-grain roughness height) is a better representative length scale for defining the extent of the roughness sublayer compared to k because of a common measure of the influence of the roughness on the mean flow. In the present study, the rod roughness has a height of $\delta/k = 20$, which is larger than the criterion of Jimenez (2004). The depth of the roughness sublayer in the present study is estimated to be about 0.25δ ($5k_s = 1.59\delta$).

Lee and Sung (2007) showed that although the turbulent Reynolds stresses normalized by the friction velocity are affected throughout the entire boundary layer, good surface similarity was observed for the Reynolds anisotropic tensor in the outer layer without normalization by the friction velocity. They proposed that the increased production of turbulent kinetic energy in the vicinity of the rough wall causes an increase in magnitude of the turbulent Reynolds stresses, but it makes no significant contribution to the relative magnitude to the each turbulent Reynolds stress components. Therefore, they assumed that the redistribution of turbulent kinetic energy for the rough-wall TBL is similar to that for the smooth-wall TBL.

To better comprehend the redistribution of turbulent energy, the pressure-strain tensors in the Reynolds stress budget equation is scrutinized in detail. The turbulent kinetic energy is mainly produced at $y^+ \approx 10$ in a smooth wall and then transferred to the interior of the flow. Although the pressure term associated with the redistribution of energy is not measurable in experimental studies, its effect is important close to the wall. The pressure-strain tensors relevant to the system examined in the present study is written as,

$$\Pi_{ij} = -p\left\langle \frac{\partial u_i}{\partial x_j} + \frac{\partial u_j}{\partial x_i} \right\rangle, \tag{4}$$

where the indices i, j are 1, 2, or 3 for the streamwise, wall-normal and spanwise directions, respectively. The profiles of the pressure-strain redistribution tensors are displayed in Fig. 4. All quantities are normalized by u_τ^4/ν. Locations II and IV marked in Fig. 1 are considered. In each plot, a vertical dashed line is used to mark the roughness crest ($y = k$). The profiles of the pressure-strain redistribution in the roughness sublayer differ significantly between the smooth and rough wall systems. Within the cavity and very near the bottom wall, turbulent kinetic energy is transferred from the vertical direction to the streamwise direction at position II and to the spanwise direction at position IV. Furthermore, above the roughness crest, turbulent energy is transferred from the streamwise direction to the vertical and spanwise directions. Near the leading edge (position IV), this energy transfer is very large and constitutes the main energy source of wall-normal and spanwise velocity fluctuations, as shown in the Reynolds anisotropic tensor. These results are consistent with those for channel flow reported by Ashrafian and Andersson (2006). However, no discernible difference in the outer coordinates (Fig. 5) is observed between the rough-wall and smooth-wall TBLs above $y/\delta = 0.45$ ($y \sim 9k$ and $y \sim 1.5k_s$), indicating that the redistribution of turbulent kinetic energy in the outer layer is similar in the systems with smooth and rough walls. This finding supports the conjecture of Lee and Sung (2007) that rod roughness does not significantly affect anisotropy tensors in the outer layer. Within the roughness sublayer, the turbulent energy is redistributed from $\langle u^{+2}\rangle$ to $\langle v^{+2}\rangle$ and $\langle w^{+2}\rangle$, and the energy transfer follows a trend similar to that observed for the smooth wall, except that its magnitude is increased to a greater degree in the roughness sublayer than in the layer adjacent to the smooth wall.

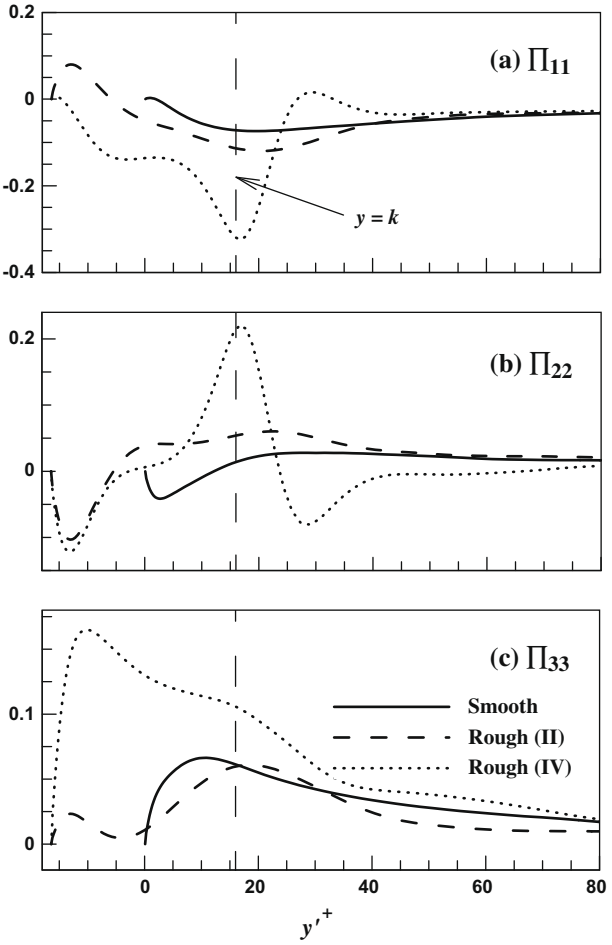

Fig. 4. Pressure-strain tensors in the inner coordinates, normalized by u_τ^4/ν.

3.4. Vorticity fluctuations

Vorticity is closely associated with turbulence production and dissipation in a wall-bounded turbulent flow (Ikeda and Durbin, 2007). Vorticity is also an important characteristic of the small-scale structure because the length scales that contribute most to the vorticity spectrum reside in the dissipative range. Vorticity statistics should therefore be useful in understanding the behavior of the small-scale structure of a rough wall. Relatively few vorticity measurements have been reported for turbulent flows over rough walls. Bhaganagar et al. (2004) studied the behavior of small-scale structures by examining vorticity fluctuations on one side wall with regular three-dimensional roughness elements. They observed that the outer-layer vorticity is nearly isotropic and of the same magnitude and no change in small-scale statistics is shown. On the other hand, experiments by Krogstad and Antonia (1994) and Shafi and Antonia (1997) on a boundary layer showed that the vorticity variances in the outer layer are slightly higher for a rough wall than for a smooth wall. Fig. 6 shows the distributions of the r.m.s. vorticity fluctuations normalized by the friction velocity for the rough and smooth walls in the outer coordinates. Above the region $y/\delta = 0.55$ ($y \sim 11k$ and $y \sim 2k_s$), the vorticity fluctuations of the rough and smooth walls collapse well and attain the same magnitude. This indicates that above the roughness region, the small-scale structures of the vortical motions are almost the

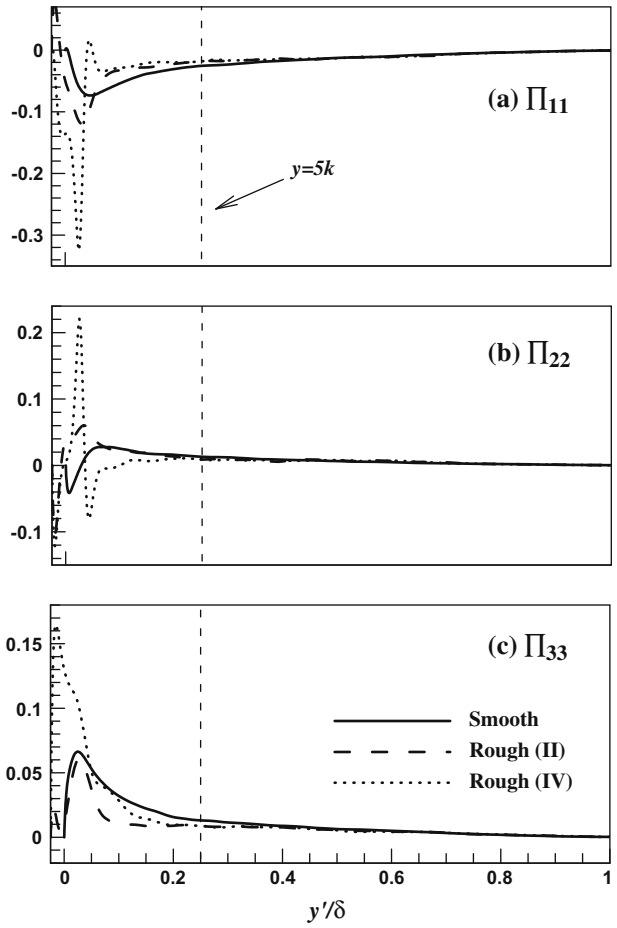

Fig. 5. Pressure-strain tensors in the outer coordinates, normalized by u_τ^4/ν.

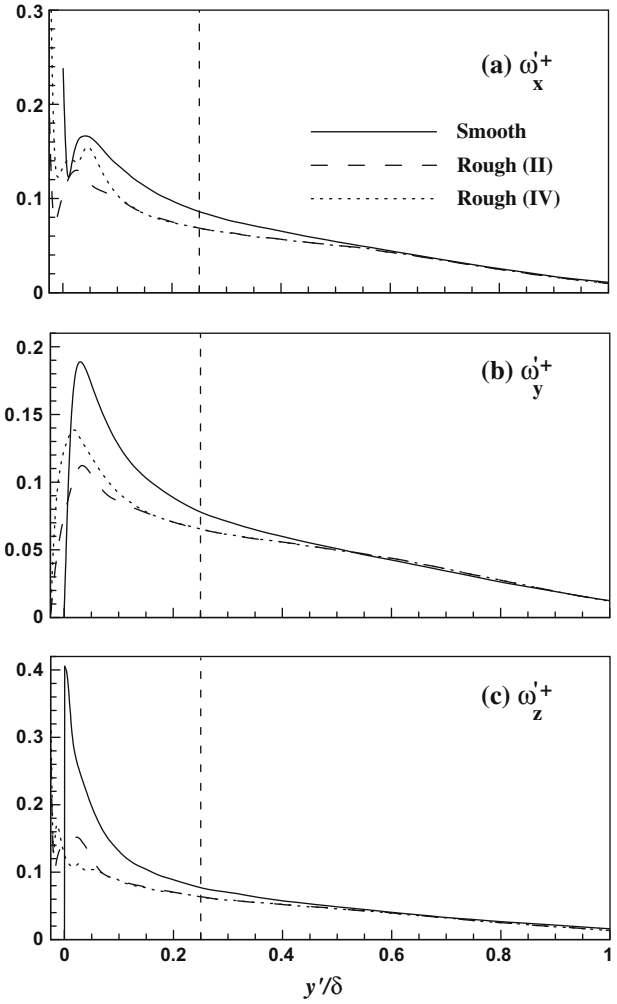

Fig. 6. Vorticity fluctuations in the outer coordinates, normalized by u_τ^2/ν.

same over the rough and smooth walls. In the roughness sublayer, however, the presence of the rod roughness causes the maximum values of the three components to be smaller for the rough wall than for the smooth wall. These findings demonstrate that in the flow past a smooth wall, in which large-scale vortices dominate, anisotropy arises rapidly and hence the vorticity fluctuations are larger in magnitude.

3.5. Quadrant analysis

A useful way of quantifying the difference between rough- and smooth-wall boundary layers is to compare the contributions to the Reynolds shear stress. The Q2 event (ejection, $u<0$, $v>0$) and the Q4 event (sweep, $u>0$, $v<0$) make larger contributions to the Reynolds shear stress than the Q1 and Q3 events. Lee and Sung (2007) investigated the velocity triple product of the wall-normal direction, which is sensitive to surface roughness, and observed a very large positive peak of the wall-normal directions over the rough wall in the roughness sublayer, indicating that the Q2 events occur very strongly in this system. Fig. 7a and b show the contributions of the Q2 and Q4 events, respectively, to the Reynolds shear stress, normalized by the local mean Reynolds shear stress. To inspect the turbulent structure in the vicinity of the rough wall, two locations over the rough wall (II and IV) and one over the smooth wall are compared. Good agreement is observed between the smooth and rough walls for both the Q2 and Q4 events above $y/\delta = 0.16$ ($y \sim 3k$ and $y \sim k_s$). These results are consistent with those of Schultz and Flack (2007), which showed outer-layer similarity for three-dimensional roughness in the form of a

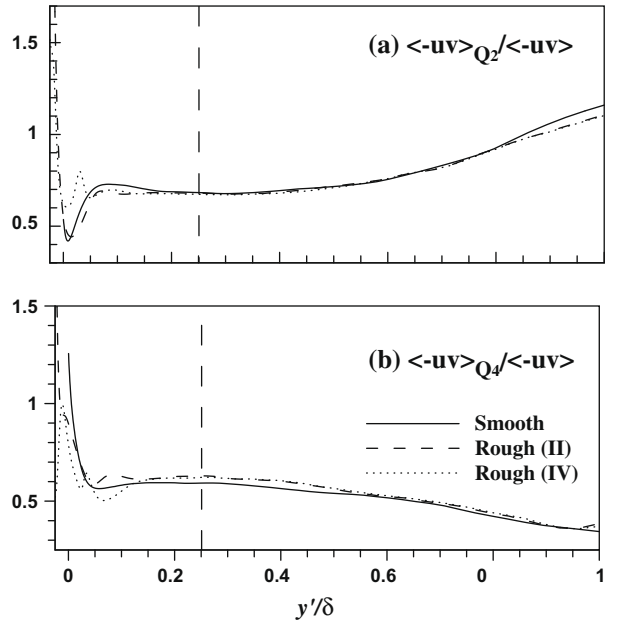

Fig. 7. Quadrant analysis in the outer coordinates, normalized by local mean Reynolds shear stress.

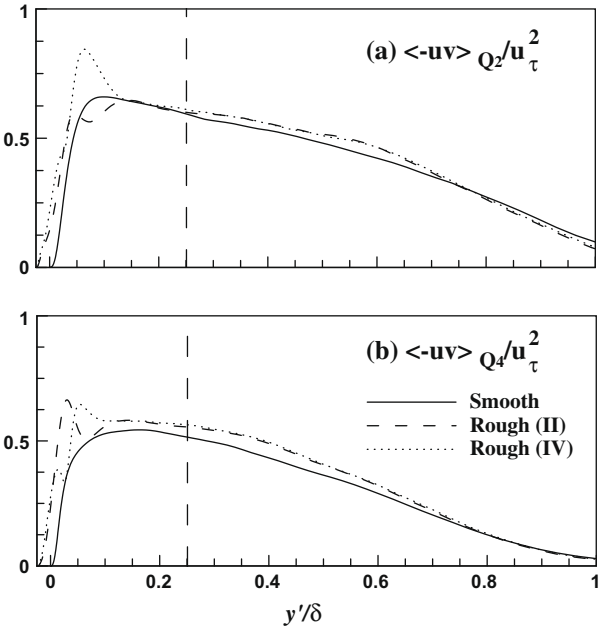

Fig. 8. Quadrant analysis in the outer coordinates, normalized by u_τ^2.

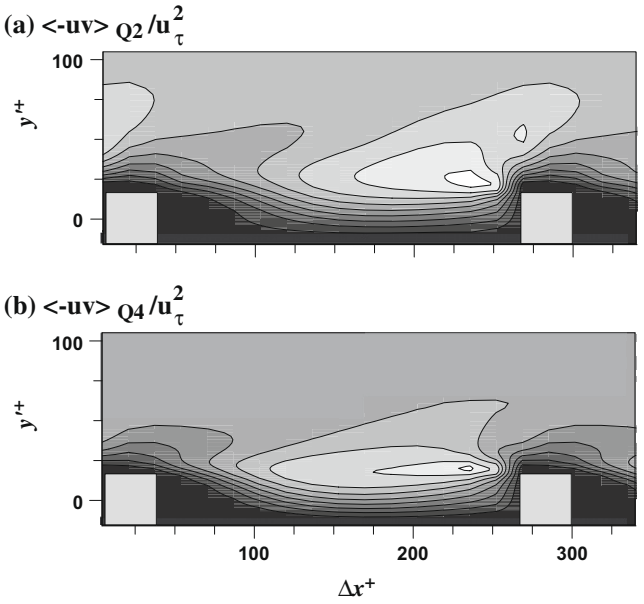

Fig. 9. Distributions of ejection and sweep motions in wall coordinates, normalized by u_τ^2.

honed pipe by investigating the percentage contributions from the ejection and sweep events. In the present study, despite the use of a roughness height of $\delta/k = 20$ ($\delta/k_s = 3.2$), good wall similarity is observed for the contributions of the Q2 and Q4 events in the outer layer for the smooth and rough walls when these variables are normalized by the local Reynolds shear stress. However, when scaled by the friction velocity, the contributions of the Q2 and Q4 events to the Reynolds shear stress in the outer layer differ between the smooth and rough-walled systems (Fig. 8). Especially, the magnitude of the Q4 event in the rough wall above the roughness sublayer is larger more than 10% compared to the magnitude in the smooth wall. This behavior is similar to that found in other experiments on TBLs over rough walls. Krogstad and Antonia (1992) observed that for most of the boundary layer, the magnitudes of the Q2 and Q4 events are larger across the whole boundary layer for a woven mesh roughness of roughness height $\delta/k_s = 15$ than for the smooth wall. These findings indicate that although the magnitudes of the Q2 and Q4 events vary not only in the roughness sublayer but also in the outer layer, the relative contributions from ejection and sweep motions in the outer layer are similar for the smooth and rough-walled systems, as was observed for the Reynolds anisotropic tensor.

To highlight the near-wall behavior of the Q2 and Q4 events, Fig. 9 depicts the distributions of the Q2 and Q4 components of the Reynolds shear stress near the roughness in the inner coordinates. We can observe that the strengths of ejection and sweep events are increased along the downstream direction from the trailing edge of rod and have a maximum value near the leading edge of rod. These increased ejection and sweep events can be explained by the rod-induced blockage effect in front of each rod and by the sweeping of a large amount of high-momentum fluid into the cavity between the surface rods.

3.6. Instantaneous flow fields

The presence of rod roughness on the surface induces substantial changes in the flow field not only within the cavities between consecutive rods, but also in a certain layer above the crests of the rods. These effects can be attributed to the vigorous ejection and sweep motions that occur in these systems, as observed in the quadrant analysis. The instantaneous flow fields within the roughness sublayer reveal the characteristics of the turbulent structure over the rough wall. Fig. 10 shows a visualization of the vortical structures near the roughness sublayer. The Galilean

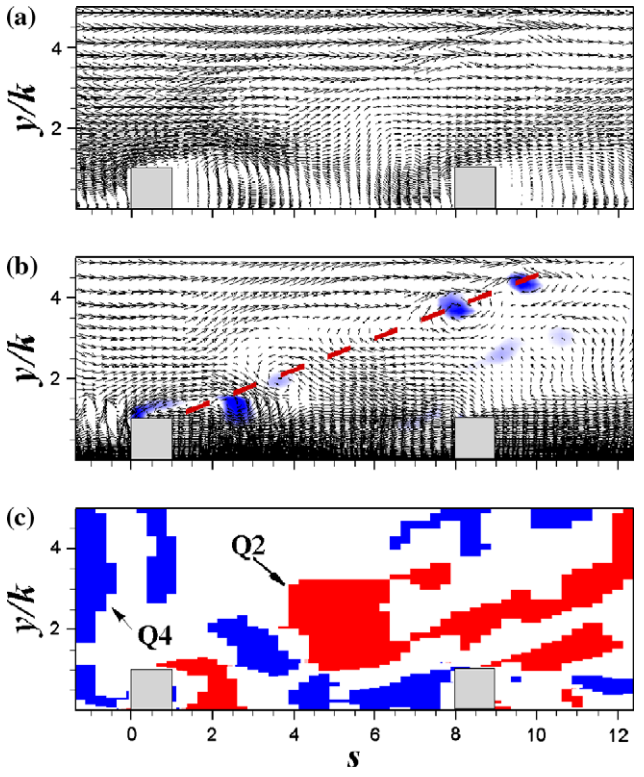

Fig. 10. Visualization of vortical structures near the roughness sublayer. (a) Instantaneous velocity vector field of (u, v) near the roughness sublayer, (b) instantaneous velocity vector field with the reference frame velocity $U_f = 0.4U_\infty$, iso-contour represents the swirling strength, and (c) spatial distribution of the Q2 and Q4 events for the same instantaneous flow field. Red and blue colors represent Q2 and Q4 events, respectively. (For interpretation of the references to color in this figure legend, the reader is referred to the web version of this article.)

decomposition technique is applied to instantaneous velocity vectors with the reference velocity $U_f = 0.4U_\infty$ in Fig. 10b (Adrian et al., 2000). Vortical structures are identified by a positive value of the swirling strength λ_{ci} (Zhou et al., 1999). Fig. 10a shows instantaneous velocity vectors (u, v) in the (x, y)-plane through the middle of the spanwise computational domain, while Fig. 10b shows the corresponding vector field of velocity fluctuations and iso-contours of vortical structures with the reference velocity $U_f = 0.4U_\infty$ in the roughness sublayer. Kline and Robinson (1989) defined a vortex as a region of concentrated vorticity around which the pattern of streamlines is roughly circular when viewed in a frame moving with the center of the vortex. Following this definition, a pattern of nearly circular streamlines that coincides with the concentrated vorticity can be discerned in Fig. 10b. The downstream regions colored light blue also contain concentrated vorticity, but their vector pattern shows only a faint circular signature because of different convection velocities. These vortices are inclined at approximately 25–26° with respect to the downstream direction. Adrian et al. (2000) observed that in the TBL over a smooth wall, large-scale structures like hairpin packets grow upwards at a mean angle of approximately 12° as they move downstream. In similar experiments, Volino et al. (2007) found angles of $13.2 \pm 2.5°$ and $15.8 \pm 3.3°$ for smooth and rough walls, respectively. A time sequence of the instantaneous flow fields shows highly disrupted vortical structures above the roughness crest, and that these structures recover rapidly with moving upwards away from the rod roughness and attain a coherence similar to that observed for the smooth wall. Fig. 10c shows the spatial distributions of the Q2 and Q4 events for the same instantaneous vector field, where the Q2 and Q4 events are indicated by red and blue colors, respectively. Consistent with Coceal et al. (2007), the Q2 and Q4 events are not randomly distributed but rather are grouped into distinct regions that are consistent with those in Fig. 9. These results indicate that large amounts of high speed fluid inrush toward the cavity region between consecutive rods, and that strong ejection motions occur near the leading edge.

Fig. 11 illustrates the contours of the streamwise velocity fluctuations at $y^+ = 5$ for flows past a smooth wall (top) and rough wall (bottom). In this figure, a blue color indicates positive velocity fluctuations. At $y^+ = 5$, the streaks are elongated on the smooth wall, indicating a coherent organized structure of low-speed streaks, whereas at the same wall-normal location the streaks look significantly different above the rough wall. Ashrafian et al. (2004) observed streaky structures in the distribution of streamwise velocity fluctuations over the rough wall, similar to those of the smooth wall, but with significantly reduced coherence in the streamwise direction and no obvious spanwise coherence.

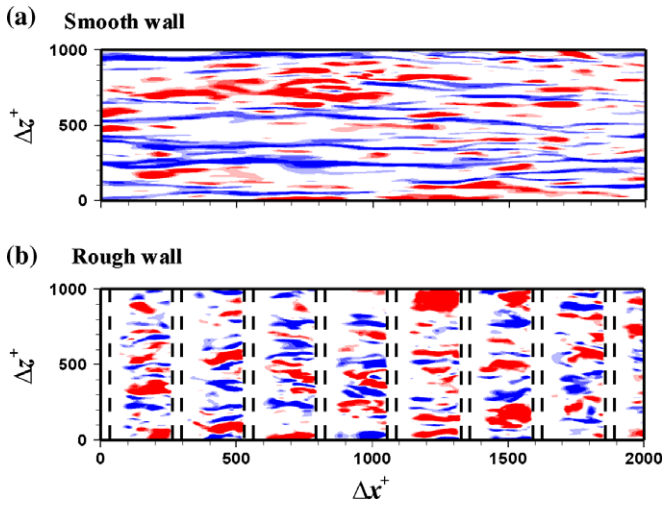

Fig. 11. Contours of streamwise velocity fluctuation at $y^+ = 5$ on the smooth wall (top) and rough wall (bottom). Red and blue colors represent high-speed ($u' > 0$) and low-speed ($u' < 0$) streaks, respectively. (For interpretation of the references to color in this figure legend, the reader is referred to the web version of this article.)

3.7. Two-point correlation

Previously, instantaneous flow fields have been used to show how turbulent structures are influenced by rod roughness within the boundary layer. However, a question remains as to whether the spatial and statistical properties of the coherent structures are similar in the outer layer of rough and smooth walls. Several previous experimental and numerical studies have elucidated the spatial characteristics of the flow past a rough wall. Using two-point correlations, Krogstad and Antonia (1994) found that introduction of a woven mesh with $\delta/k_s = 15$ onto a smooth wall caused a substantial decrease of the average extent of the streamwise two-point correlations both in the roughness sublayer and in the outer layer. This was due to a drastic increase in the inclination angle of turbulent structures in the streamwise and wall-normal planes in the TBL of the rough wall. On the other hand, recent laser-Doppler velocimetry (LDV) and particle image velocimetry (PIV) measurements over a woven mesh surface ($\delta/k = 71$) and over a smooth wall by Volino et al. (2007) showed excellent agreement, both qualitatively and quantitatively, between the turbulent structures in the spectra of the fluctuating velocity components, swirl strength, and two-point auto- and cross-correlations of the fluctuating velocity and swirl. The DNS study by Bhaganagar et al. (2004) in an asymmetric turbulent channel with three-dimensional roughness showed an increase of the streak spacing from 100 (smooth) to 140 (rough) and the average diameter of the near-wall quasi-streamwise vortices is increased from 20 (smooth) to 45 (rough) in wall units. In the study of Leonardi et al. (2003, 2004) performed in an asymmetric channel with two-dimensional rod roughness, the spatial coherence is reduced in the streamwise direction as the pitch between consecutive rods increases and the spanwise size of the streaky structures is increased in comparison with that of smooth wall.

In the present study, we examined the auto-correlation of velocity fluctuations to investigate the spatial character over the rough wall. The two-point correlation of velocity fluctuations as a function of streamwise and spanwise spatial separations is defined as:

$$R_{ij}(\Delta x, y', \Delta z; x_{ref}, y_{ref}) = \frac{\langle u_i(x_{ref}, y_{ref}, z) u_j(x_{ref} + \Delta x, y', z + \Delta z) \rangle}{\sqrt{\langle u_i^2(x_{ref}, y_{ref}) \rangle} \sqrt{\langle u_j^2(x_{ref} + \Delta x, y') \rangle}}, \quad i, j = 1, 2, 3 \tag{5}$$

where x_{ref} and y_{ref} denote the reference positions in the streamwise and wall-normal directions and the subscripts i and j are the corresponding Cartesian coordinates. As shown in Fig. 12, we compared two-point correlations of the streamwise and wall-normal velocity fluctuations separated in the spanwise direction $R_{ij}(\Delta z)$ at $y^+ = 5$. The separation distance is normalized by local wall units. The two-point correlation of the streamwise velocity R_{uu} shows that the streak spacing is 150 wall units for the rough wall, whereas 100 for the smooth wall. Moreover, the two-point correlation of the wall-normal velocity fluctuations shows that the average diameter of the near-wall streamwise vortices at $y^+ = 5$ is increased from 25 for the smooth wall to 65 for the rough wall due to the blockage effect of the roughness which induces the transfer of wall-normal velocity component to the wall-normal and spanwise directions. These findings indicate that introduction of the rod roughness elements onto the smooth wall increases the average streak spacing

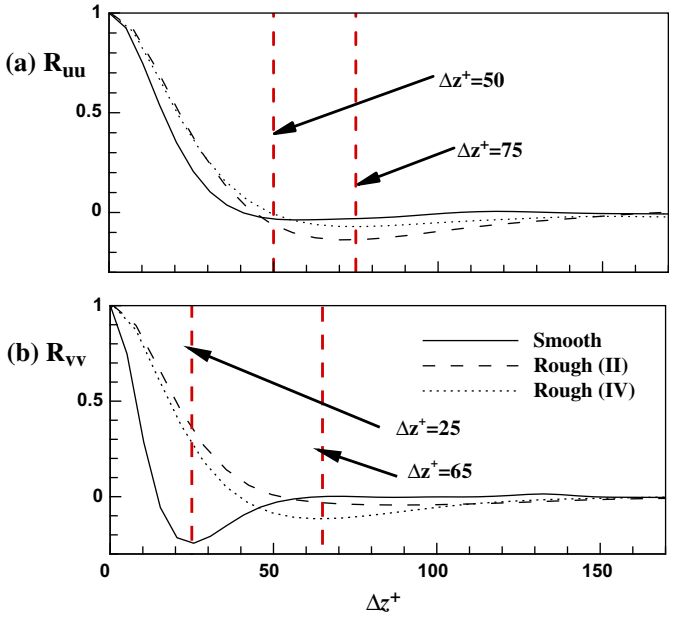

Fig. 12. Two-point spanwise correlations of streamwise and wall-normal velocity fluctuation with the separation distance normalized by the friction velocity at wall-normal location of $y^+ = 5$.

in the spanwise direction, and also the diameter of the streamwise vortices. These are consistent with the previous DNS results in the turbulent channel flow (Leonardi et al., 2003, 2004; Bhaganagar et al., 2004).

Fig. 13 shows contour plots of the two-point correlations of the streamwise velocity fluctuations R_{uu} at both $y^+_{ref} = 50$ and $y_{ref}/\delta = 0.5$ in the (x, y)-plane. The contours of constant correlation magnitude are roughly elliptical in shape with the major axis tilted at an angle to the streamwise direction. The streamwise two-point correlations for the smooth and rough walls in the outer layer are in quantitative agreement, as shown in Fig. 13c and d. The mean inclination angle of $R_{uu} = 0.3$ is about 11–12° and the shape of the contours is almost the same. In the experimental study over the three-dimensional mesh by Krogstad and Antonia (1994), however, the mean inclination angle of the $R_{uu} = 0.3$ contour had an average value of about 10° for the smooth wall and a much larger value of about 38° for the rough wall at $y/\delta = 0.16$. In the roughness sublayer, marked differences are observed between the smooth- and rough-wall boundary layers. The contour of two-point correlations $R_{uu} = 0.3$ indicates that the average extent of the streamwise two-point correlation decreases and the angle of inclination of R_{uu} significantly increases due to the rod roughness. The contour of R_{uu} is inclined at an average angle of about 26° with respect to the rough wall compared to about 13–14° with respect to the smooth wall. In the DNS studies of the turbulent channel flow over rough wall, Coceal et al. (2007) found that the mean angle with respect to the wall decreased sharply with height from 21.6° at the top of the roughness ($y = k$) to 14.4° at $y = 1.5k$, then decreased more slowly thereafter to a value of 12.2° at $y = 2.75k$. Leonardi et al. (2004) showed that a decreased streamwise coherence, relative to the smooth wall, is observed for rough wall and the inclination is increased.

Fig. 14 displays the contours of the two-point correlation of the wall-normal velocity fluctuations R_{vv} at $y^+_{ref} = 50$ and $y_{ref}/\delta = 0.5$. Although the trend in the auto-correlations of the wall-normal velocity for the rough wall is similar to that for the smooth wall at $y_{ref}/\delta = 0.5$, structural differences exist between the rough and smooth wall systems at $y^+_{ref} = 50$. In the roughness sublayer, the roughness induces more elongated structures along the wall-normal direction owing to the less efficient damping of vertical motions near the surface roughness.

3.8. Conditionally averaged flow fields

Both the quadrant analysis results and the two-point correlation data provide evidence of organized motions in the TBL above the rough wall. In the present study, since we are interested in changes in the turbulent structures induced by introducing rod roughness onto a smooth wall, it is useful to study the effects of three-dimensional flow structures on Reynolds shear stress-producing events. To better comprehend the modification of the flow

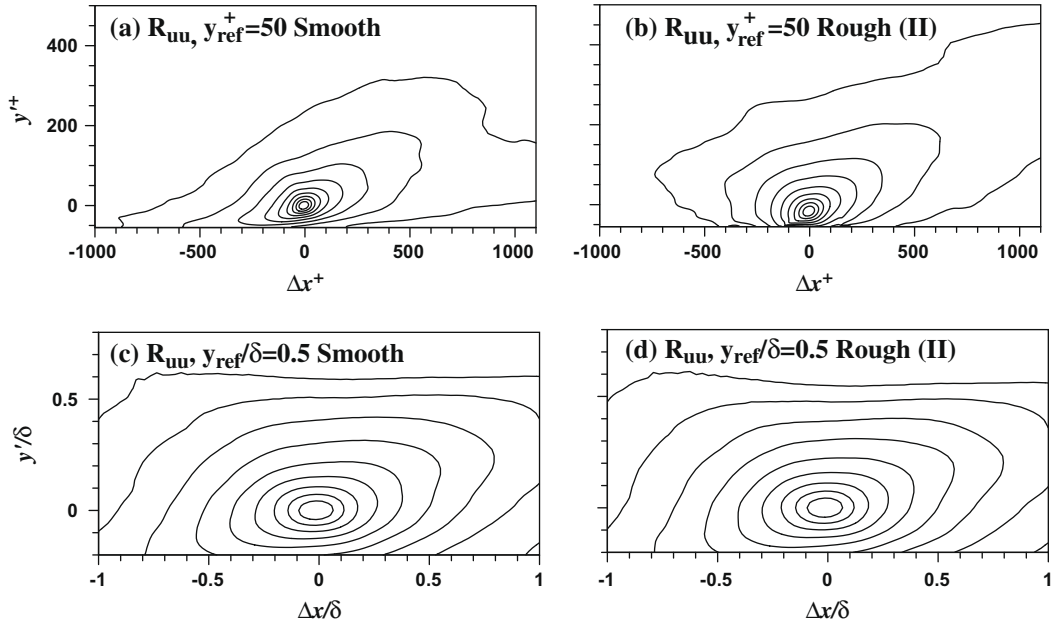

Fig. 13. Contours of R_{uu} in the (x, y)-plane, contour magnitudes of R_{uu} vary from 0.1 to 0.9. (a) Smooth wall $y^+ = 50$, (b) rough wall $y^+ = 50$, (c) smooth wall $y/\delta = 0.5$, and (d) rough wall $y/\delta = 0.5$.

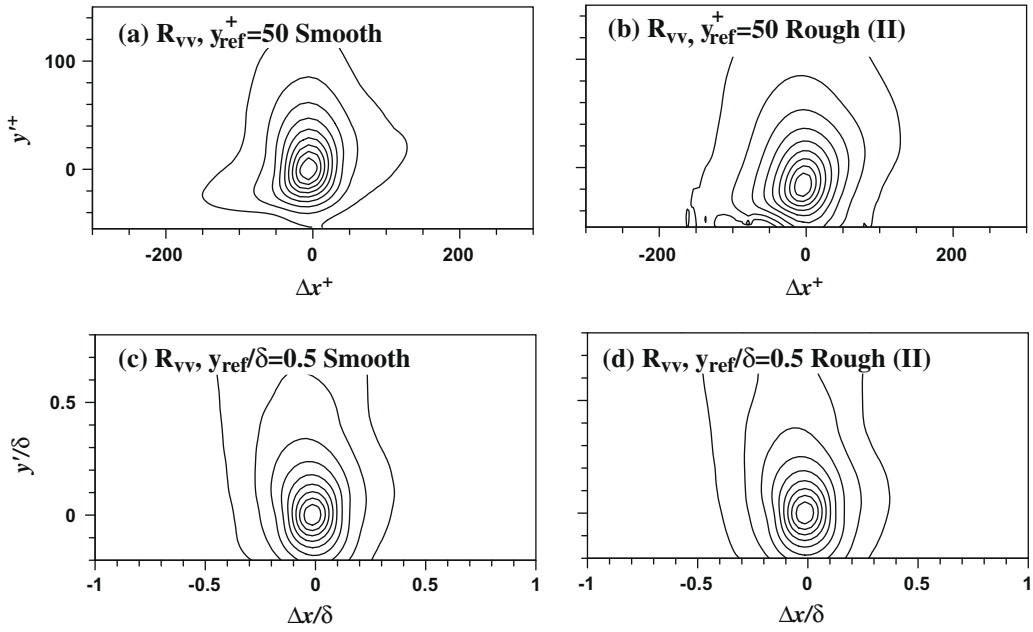

Fig. 14. Contours of R_{vv} in the (x, y)-plane, contour magnitudes of R_{vv} vary from 0.1 to 0.9. (a) Smooth wall $y^+ = 50$, (b) rough wall $y^+ = 50$, (c) smooth wall $y/\delta = 0.5$, and (d) rough wall $y/\delta = 0.5$.

structures to Reynolds stress-producing events, we examined the conditionally averaged flow field around these structures. Through an appropriate choice of the event (or condition), a conditionally averaged flow field can be obtained. However, from a statistical standpoint, it is very hard to obtain the true converged conditional average when the condition is multi-dimensional and strong perturbations exist near the wall. Thus, we approximate the conditionally averaged flow field by linear stochastic estimation (LSE) (Adrian, 1996). The conditional average of a fluctuating flow field $g_i(\boldsymbol{x}, t)$, given events or conditions, $E_j(\mathbf{x}'_j, t)$ ($j = 1, \ldots, N$, where N is the total number of conditions specified at the point $\mathbf{x}'_j$) is denoted by $\langle g_i|\mathbf{E}\rangle$. Given $E_j(\mathbf{x}'_j, t)$, the conditional average is the best estimate for $g_i(\boldsymbol{x}, t)$, in the sense of minimum mean square error. The linear stochastic approximation of the conditional average $\langle g_i|\mathbf{E}\rangle$ is written as,

$$\hat{g}_i(x,t) = L_{ij}(x,x'_j)E_j(x'_j,t) \tag{6}$$

Choosing L_{ij} to minimize the mean square error yields equations for L_{ij} in terms of uncorrelated, two-point, second-order correlation tensors:

$$\langle E_j(x'_j)E_k(x'_k)\rangle L_{ij} = \langle g_i(x)E_k(x'_k)\rangle \tag{7}$$

where the angle brackets represent the ensemble average. The accuracy of linear stochastic estimation as an approximation to the conditional average has been reported elsewhere.

It is well known that near-wall vortical structures are closely associated with the production of Reynolds shear stress. The organized structures in turbulent channel flow can be estimated based on the event that makes dominant contributions to the Reynolds shear stress (Moin et al., 1987). In turbulent flow over a rough wall, experimental and numerical results show that the Reynolds shear stress increases significantly due to the surface roughness. We examined the change in the vortical structures associated with the increased Reynolds shear stress over the rod-roughened wall. At any given distance from the wall (y'), an event of the conditional average is chosen as the Q2 and Q4 quadrant events that maximize the contribution to the Reynolds shear stress. These events (u_m, v_m) are obtained from the maximum value of the probability weighted Reynolds shear stress $-uv\, f_u(u, v)$. Fig. 15 displays the inclination angle $\gamma_{II,IV} = \tan^{-1}(v_m/u_m)$ of the Q2 and Q4 event vectors that maximize the contribution to the Reynolds stress over two locations II and IV. These profiles show substantial differences between the rough- and smooth-walled systems within the roughness sublayer. Over the rough wall, especially near the leading edge (location IV), the inclination angle of the ejection motions is much larger than that over the smooth wall due to the blockage effect of surface roughness. On the other hand, the profiles of the inclination angle of the Q2 and Q4 event vectors collapse well above $y/\delta = 0.25$ ($y \sim 5k$ and $y \sim k_s$) for both smooth and rough walls. The characteristics of the Q2 and Q4 events most contributing to the Reynolds shear stress are similar between rough- and smooth-walls in the outer layer.

In the turbulent boundary layer over the smooth wall, it is well known that the flow structures associated with the Q2 event are a counter-rotating pair of streamwise vortices very near the wall that induces ejection motion between the vortices, and hairpin structures further away from the wall (Adrian et al., 2000). Lee et al. (2008) observed a series of vortices above the rod roughness moving upward with an inclination angle. They proposed that these vortices induced by the rod roughness are similar to hairpin structures and the heads of hairpin vortices are located at $y = 4$–$5k$. They also showed the vortices moving downward in the cavity between two rods. In the present DNS, we also observed similar patterns of vortical structures in the instantaneous flow field as discussed in the previous section. To observe the vortical structures associated with the Q2 event more clearly, we investigated conditionally averaged flow fields by using LSE and represent them in Figs. 16 and 17. Near-wall vortical structures are depicted by iso-surfaces of the swirling strength λ_{ci} computed from the conditionally averaged velocity field with the condition of (u_m, v_m) for the Q2 events at the location II with different y locations ($y^+_{ref} = 50$ and $y_{ref}/\delta = 0.5$) over the rough and smooth walls. To exclude the mean shear effects induced by the surface roughness, the velocity fluctuation components are used for calculating the swirling strength. The level of iso-surface is chosen as 30% of the maximum value of λ_{ci} at each wall-normal location. The arrows represent the velocity events used in the estimation. Since the

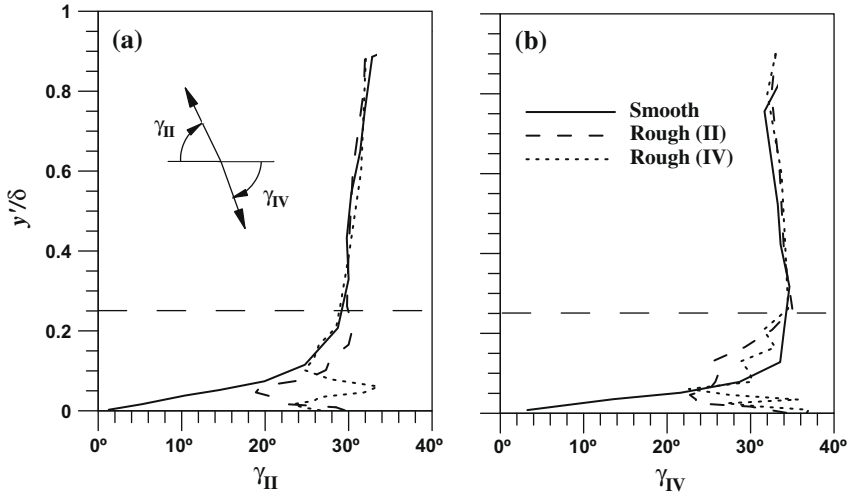

Fig. 15. Angles of the Q2 and Q4 quadrant event vectors which make the maximum contribution to local Reynolds shear stress.

results of the Q4 event are similar to those of the Q2 event (not shown here), we only compared the results of the Q2 event in Figs. 16 and 17.

In Fig. 16, we can observe hairpin-like vortical structures near the rough and smooth walls ($y^+ = 50$). For the rough wall, a

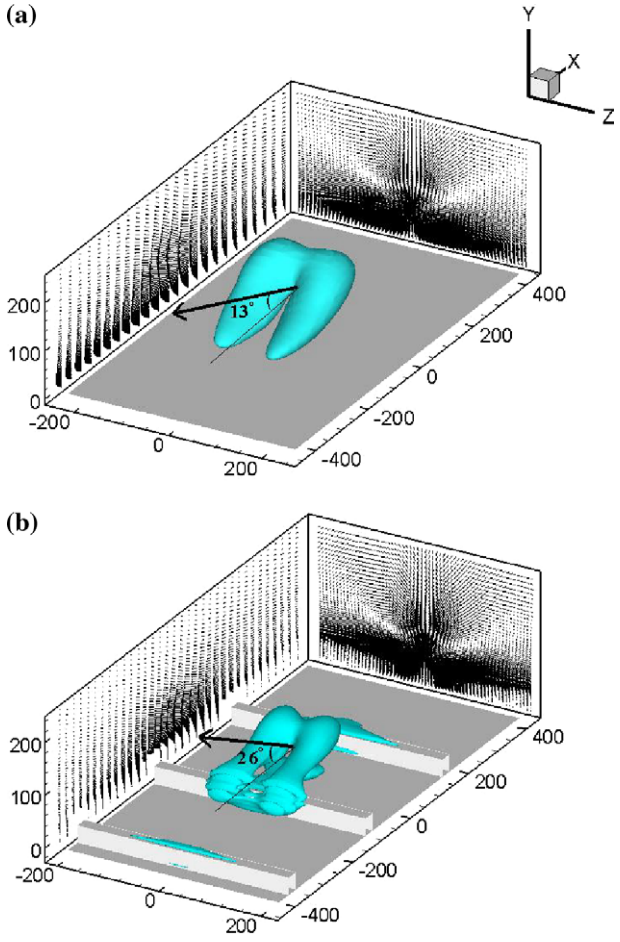

Fig. 16. Conditionally averaged vortical structure and velocity vectors fields extracted from a Q2 event maximizing the Reynolds shear stress at location II and $y^+_{ref} = 50$. Iso-surface represents λ_{ci} with the 30% contour level of the maximum value. The velocity vectors show the conditionally averaged in-plane velocity fluctuations. (a) Smooth wall and (b) rough wall.

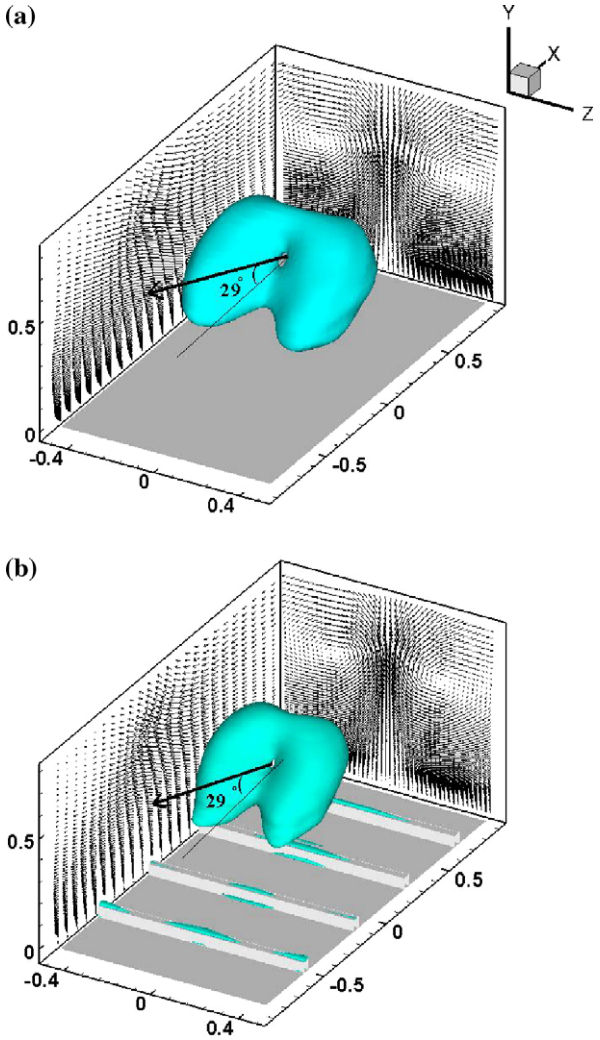

Fig. 17. Conditionally averaged vortical structure and velocity vectors fields extracted from a Q2 event maximizing the Reynolds shear stress at location II and $y_{ref}/\delta = 0.5$. Other conditions are the same as in Fig. 16a smooth wall and Fig. 16b rough wall.

low-momentum zone exists between two legs and beneath hairpin head at $y^+ \sim 100$ ($y \sim 3.5k$). The DNS study of channel flow by Ashrafian and Andersson (2006) yielded similar results; although the mean flow and the turbulence statistics are dramatically affected by the rods within the roughness sublayer, the streamwise vortical structures are observed above the rods. However, the hairpin vortical structure in the present study is significantly changed near the wall due to the surface roughness. In the roughness sublayer at $y^+_{ref} = 50$, the streamwise length scale is shortened as compared with the smooth wall. Moreover, the distributions of vector fields associated with the Q2 event in the (x, y) and (x, z)-planes are disturbed by the reduced damping of the wall-normal velocity fluctuations close to the rough wall and by the break-up of structures. Compared to the smooth wall, the vector fields related to the ejection motions over the rough wall are widely distributed along the wall-normal direction and the magnitude of the Q2 event is larger. This is consistent with the observation of Lee and Sung (2007) who found a very large positive peak of the velocity triple product for the rough wall, indicative of very strong ejection events.

In Fig. 17, we examined the conditionally averaged flow structures with the Q2 event specified above the roughness sublayer between rough and smooth walls ($y_{ref}/\delta = 0.5$). The characteristics of the velocity field and vortical structure of the rough wall are very similar to those of the smooth wall. The vortical structures associated with the Reynolds shear stress in the outer layer of the rough wall has almost the same geometrical shape as those in the smooth wall although the Reynolds shear stress differs in magnitude between the rough and smooth walls. This is consistent well with the experimental result of Volino et al. (2007) who demonstrated that the two-point correlations of various quantities and the average angles of maximum correlation are in quantitative agreement between the smooth and rough walls in the region above the roughness sublayer.

4. Conclusions

Instantaneous flow fields of the DNS of Lee and Sung (2007) were used to elucidate the effects of surface roughness on a TBL. The roughness elements employed were periodically arranged two-dimensional spanwise rods, and the roughness height was $k/\delta = 0.05$. The Reynolds number based on the momentum thickness is $Re_\theta = 1351$ for rough wall and $Re_\theta = 1098$ for smooth wall, respectively. We found that introduction of these roughness elements onto the smooth wall affected the Reynolds stresses throughout the entire boundary layer when normalized by the friction velocity, but that vorticity fluctuations in the outer layer were only mildly affected. These findings indicated that the structure of small-scale turbulence characteristics such as vorticity fluctuations is similar for smooth and rough walls, whereas turbulent stresses acting over a large scale are affected in the outer layer. Inspection of the pressure-strain tensors, which are independent of the estimated friction velocity, disclosed that despite the increased Reynolds stresses in the vicinity of the rough wall compared to the smooth wall, the redistribution of turbulent energy over the rough wall is very similar to that of the smooth wall in the outer layer. Consistent with this, quadrant analysis revealed that while the Q2 and Q4 events normalized by the friction velocity exhibited a lack of wall similarity, good wall similarity for the Q2 and Q4 events was observed in the outer layer when normalized by the local mean Reynolds shear stress. These findings demonstrate that the outer-layer similarity between rough and smooth walls depends on the scaling parameter and turbulent statistics used. Although the magnitudes of the turbulent intensities are larger for the rough wall than for the smooth wall, the relative magnitudes of the Q2 and Q4 events were similar for the rough and smooth walls in the outer layer. Conditional averaging was carried out to investigate the turbulent vortices associated with the production of Reynolds shear stress by using linear stochastic estimation. The conditionally averaged flow fields for the Reynolds-stress-maximizing Q2/Q4 events showed that the near-wall vortical structures were significantly lifted up and shortened in the streamwise direction by the surface roughness. The ejection motion was strongly induced by the blockage effect of the surface roughness, and the surface rods affected not only the magnitude but also the distribution of the swirling strength. Similar results were obtained from the distributions of joint weighted probability density function for maximizing the Reynolds shear stress. However, compared to the smooth-wall TBL, no discernible structural differences exist in the outer layer. These findings illustrate that introduction of surface roughness elements onto the smooth surface did not significantly affect the turbulent vortices producing Reynolds stresses in the outer layer.

Acknowledgement

This work was supported by the Creative Research Initiatives of MEST/KOSEF and partially supported by KISTI under the Strategic Supercomputing Support Program.

References

Adrian, R.J., 1996. Stochastic estimation of the structure of turbulent fields. In: Bonnet, J.P. (Ed.), Eddy Structure Identification. Springer, pp. 145–196.
Adrian, R.J., Meinhart, C.D., Tomkins, C.D., 2000. Vortex organization in the outer region of the turbulent boundary layer. Journal of Fluid Mechanics 422, 1–54.
Ashrafian, A., Andersson, H.I., 2006. Roughness effects in turbulent channel flow. Progress in Computational Fluid Dynamics 6, 1–20.
Ashrafian, A., Andersson, H.I., Manhart, M., 2004. DNS of turbulent flow in a rod-roughened channel. International Journal of Heat and Fluid Flow 25, 373–383.
Bhaganagar, K., Kim, J., Coleman, G., 2004. Effect of roughness on wall-bounded turbulence. Flow, Turbulence and Combustion 72, 463–492.
Coceal, O., Dobre, A., Thomas, T.G., 2007. Structure of turbulent flow over regular arrays of cubical roughness. Journal of Fluid Mechanics 589, 375–409.
Flack, K.A., Schultz, M.P., Shapiro, T.A., 2005. Experimental support for Townsend's Reynolds number similarity hypothesis on rough walls. Physics of Fluids 17. Article #035102.
Flack, K.A., Schultz, M.P., Connelly, J.S., 2007. Examination of a critical roughness height for outer layer similarity. Physics of Fluids 19. Article #095104.
Ikeda, T., Durbin, P.A., 2007. Direct simulations of a rough-wall channel flow. Journal of Fluid Mechanics 571, 235–263.
Jimenez, J., 2004. Turbulent flows over rough walls. Annual Review of Fluid Mechanics 36, 173–196.
Kim, J., Kim, D., Choi, H., 2001. An immersed boundary finite-volume method for simulations of flow in complex geometries. Journal of Computational Physics 171, 132–150.
Kim, K., Baek, S.-J., Sung, H.J., 2002. An implicit velocity decoupling procedure for the incompressible Navier–Stokes equations. International Journal for Numerical Methods in Fluids 38, 125–138.
Kline, S.J., Robinson, S.K., 1989. Quasi-coherent structures in the turbulent boundary layer, Part 1: status report on a community-wide summary of the data. Near Wall Turbulence 218, 247.
Krogstad, P.-Å., Antonia, R.A., 1992. Comparison between rough- and smooth-wall turbulent boundary layers. Journal of Fluid Mechanics 245, 599–617.
Krogstad, P.-Å., Antonia, R.A., 1994. Structure of turbulent boundary layers on smooth and rough walls. Journal of Fluid Mechanics 277, 1–21.
Krogstad, P.-Å., Antonia, R.A., 1999. Surface roughness effects in turbulent boundary layers. Experiments in Fluids 27, 450–460.
Krogstad, P.-Å., Andersson, H.I., Bakken, O.M., Ashrafian, A., 2005. An experimental and numerical study of channel flow with rough walls. Journal of Fluid Mechanics 530, 327–352.
Lee, S.-H., Sung, H.J., 2007. Direct numerical simulation of turbulent boundary layer over a rod-roughened wall. Journal of Fluid Mechanics 584, 125–146.
Lee, S.-H., Kim, J.H., Sung, H.J., 2008. PIV measurements of turbulent boundary layer over a rod-roughened wall. International Journal of Heat and Fluid Flow 29, 1679–1687.
Leonardi, S., Orlandi, P., Smalley, R.J., Djenidi, L., Antonia, R.A., 2003. Direct numerical simulations of turbulent channel flow with transverse square bars on one wall. Journal of Fluid Mechanics 491, 229–238.
Leonardi, S., Orlandi, P., Djenidi, L., Antonia, R.A., 2004. Structure of turbulent channel flow with square bars on one wall. International Journal of Heat and Fluid Flow 25, 384–392.

Lund, T.S., Wu, X., Squires, K.D., 1998. Generation of turbulent inflow data for spatially-developing boundary layer simulation. Journal of Computational Physics 140, 233–258.

Moin, P., Adrian, R.J., Kim, J., 1987. Stochastic estimation of organized structures in turbulent channel flow. In: Proceedings of the 6th Turbulent Shear Flow Symposium, pp. 16.9.1–16.9.8.

Orlandi, P., Leonardi, S., 2006. DNS of turbulent channel flows with two- and three-dimensional roughness. Journal of Turbulence 7, 1.

Orlandi, P., Leonardi, S., 2008. Direct numerical simulation of three-dimensional turbulent rough channels: parameterization and flow physics. Journal of Fluid Mechanics 606, 399–415.

Raupach, M.R., Antonia, R.A., Rajagopalan, S., 1991. Rough-wall boundary layers. Applied Mechanics Reviews 44, 1–25.

Sabot, J., Saleh, I., Comte-Bellot, G., 1977. Effects of roughness on the intermittent maintenance of Reynolds shear stress in pipe flow. Physics of Fluids 20, 150–155.

Schultz, M.P., Flack, K.A., 2005. Outer layer similarity in fully rough turbulent boundary layers. Experiments in Fluids 38, 328–340.

Schultz, M.P., Flack, K.A., 2007. The rough-wall turbulent boundary layer from the hydraulically smooth to the fully rough regime. Journal of Fluid Mechanics 580, 381–405.

Shafi, H.S., Antonia, R.A., 1997. Small-scale characteristics of a turbulent boundary layer flow over a rough wall. Journal of Fluid Mechanics 342, 263–293.

Shockling, M.A., Allen, J.J., Smits, A.J., 2006. Roughness effects in turbulent pipe flow. Journal of Fluid Mechanics 564, 267–285.

Townsend, A.A., 1976. The Structure of Turbulent Shear Flow. Cambridge University Press, Cambridge.

Volino, R.J., Schultz, M.P., Flack, K.A., 2007. Turbulence structure in rough- and smooth-wall boundary layers. Journal of Fluid Mechanics 592, 263–293.

Zhou, J., Adrian, R.J., Balachandar, S., Kendall, T.M., 1999. Mechanisms for generating coherent packets of hairpin vortices. Journal of Fluid Mechanics 387, 353–396.